Applied Catalysis B: Environmental 330 (2023) 122571

Contents lists available at ScienceDirect

Applied Catalysis B: Environmental

journal homepage: www.elsevier.com/locate/apcatb

Probing the fast transformation mechanism of Cr (VI) on carbon dots with structural defects and surface oxygen functional groups

Zhelun Pan [a,1], Ting Zhang [a,1], Xufang Qian [a,b,*], Yixin Zhao [a,b]

[a] School of Environmental Science and Engineering, Shanghai Jiao Tong University, 800 Dongchuan Rd., Shanghai 200240, China
[b] Shanghai Institute of Pollution Control and Ecological Security, Shanghai 200092, China

ARTICLE INFO

Keywords:
Carbon dots
Structural defects
Surface oxygen functional groups
Cr(VI) oxyanions
Electron transfer

ABSTRACT

Carbon dots (CDs) with dimensional size less than 10 nm have similar constitutional units to black carbon (BC) in natural environment. Herein, we investigated the fast transformation mechanism of Cr (VI) oxyanions on CDs with structural defects and surface oxygen functional groups. The electrons transferred from CDs to reduce Cr (VI) were calculated to be 0.07–0.1 mmol g^{-1} in 20 min The reduction kinetics rate driven by carbon defects is of approximately 3–5 times faster than that driven by surface oxygen-containing functional groups. Metal cations (K^+, Na^+, Ca^{2+}, Mg^{2+}) in water matrix showed negligible effect on the reduction of Cr (VI), while iron ions chelate with CDs to form a CD-COOFe complex structure, promoting diffusion and electron transfer simultaneously, enhancing the electron transfer rate constant from 6.94 × 10^{-3} to 10.00 × 10^{-3} cm s^{-1}.

1. Introduction

Carbon dots (CDs) contain carbon nuclei formed by more than 60–70 % carbon elements (mainly sp2 hybridization). Carbon nuclei cannot maintain the integrity of the graphitic structure with hexagonal network in the process of preparation, resulting in various defect sites including non-six membered rings, edges, vacancy, dopants and oxygen functional groups etc. [1,2]. These defects are very complicated which probably changed the physicochemical properties of graphitic structures. The above-mentioned defects are the primary active sites for chemical reactivity [2–5]. Defect sites break the equilibrium distribution of free electrons in graphitic structures, and the delocalized π-electron systems are formed. For example, a larger curvature effect was found in the case of CNT [6,7]. Change from uniform distribution to localized aggregation (localized π-electron system) gives it catalytic activity [4,5,8,9]. The defects of carbon nanomaterials have shown engaging catalytic performances in water treatment fields. For example, a defective oxygen-functionalized multi-walled carbon nanotubes (dCNTs) was proved to be outperformed bare CNTs (bCNTs) in activating PMS for the treatment of organic pollutants [10]. The Fenton-like catalyst Fe_2O_3@FCNT-H showed remarkably higher degradation activity (22.5 times faster) toward organic pollutant than its nonconfined analog [11]. N-doped CNTs facilitate the mediated electron transfer from phenol to PMS by a nonradical N-CNT−PMS* complexes intermediate, and it boosts organic oxidation efficiency via an electron-transfer mechanism [12,13].

The incomplete burning of biomass and fuels would lead to a wide diffusion of black carbon (BC) at microscale or even nanoscale, which accounts for around 2–18 % of annual carbon dioxide production as well as a huge proportion of missing carbon in the previous carbon cycle simulation [14–16]. BC particles with sizes smaller than 0.45 or 0.7 μm and even dissolved part are ubiquitous which could undoubtedly contribute to a substantial electron flux in the environmental chemical cycle [17–19]. Present studies have been mostly carried out on biochar, which also owns uncertainty in active centers, resulting in the difficulty in research [20]. BC particles, especially the dissolved part, possess very similar graphitic microcrystalline structure to CDs. Therefore, CDs which own uniform properties and no impurity as well as found to be critical parts of carbon materials, would be a reasonable choice in analyzing the electron transfer mechanism of BC [21].

Up to now, most of the studies have focused on the redox phenomena in the presence of BC particles, and the surface groups such as hydroquinone-like groups, which were widely used for explaining the electron donor-acceptor carriers, have been proven to be not the only contributory. Sun et al. found that the graphite structure itself can act as an intermediate for electrons, storing and releasing electrons, and its

* Corresponding author at: School of Environmental Science and Engineering, Shanghai Jiao Tong University, 800 Dongchuan Rd., Shanghai 200240, China.
E-mail address: qianxufang@sjtu.edu.cn (X. Qian).
[1] Equally contributed to this work.

https://doi.org/10.1016/j.apcatb.2023.122571
Received 28 January 2023; Received in revised form 28 February 2023; Accepted 3 March 2023
Available online 4 March 2023

electron transfer speed far exceeds that of surface functional groups [22]. Same phenomena were also obtained in the light-derived cases for the photocatalytic activity of BC and CDs [23]. Recently, we found that the unpaired electrons in the defects of carbon quantum dots (CQDs) and the carboxylic groups at the edge complexing with ferric ions showed outstanding Fenton-like catalytic activity in reductive cleavage of H_2O_2 to •OH in dark conditions [24]. Carbon defects have been widely studied as the driving force of carbon catalysis in chemical synthesis, electrochemistry, etc. [25]. However, the role in environmental-related topics is still limited. Considering preceding thorough research on cations represented by iron, metal existing in the form of anions with different valence states was set as the electron acceptor [24]. Chromium, as a typical metal-oxygen anion, is a highly toxic carcinogen due to its easy mobility across the cell membrane and strong oxidation potential. Cr (VI) oxyanions are the highest oxidation states and are representative electron acceptors in the natural environment [26,27]. The transformation mechanism of Cr (VI) to less toxic Cr (III) in the presence of carbonaceous materials is crucial from an environmental risk perspective.

In this paper, the transformation mechanism of Cr (VI) oxyanions on CDs is investigated and discussed without light interference. We explored the electron-donating properties of CDs on Cr (VI) reduction in terms of kinetics and electron transfer rate constants. Through reduction performance and electrochemical analysis, we probed into the influence factors and looked up the explanations to clarify the transformation mechanism of Cr (VI) on CDs. In light of the findings presented above, we proposed that the structural defects and surface oxygen functional groups were responsible for the driving force behind the transformation mechanism of Cr (VI), and the electric double layer significantly impacted reduction kinetics.

2. Experimental section

2.1. Materials

Detailed information of chemicals used are provided in Supporting information. All chemicals were used as received without further purification. CDs colloidal solution was prepared by an electrochemical exfoliation method [28]. Two commercial graphite rods (99.99 %) were inserted into 500 mL pure water with 6.0 cm distance, and static potentials of 30 V were applied to the two graphite electrodes by direct current power supply. After ~ 72 h with constant stirring, the transparent solution changed into a homogenous dark-yellow solution. Then, the obtained solution was filtered with 0.22 μm PTFE syringe filter and centrifuged at 15,000 rpm for 40 min to remove the large graphite particles. Finally, the CDs colloid solution was obtained. Similarly, CDs in simulated groundwater (CDSG) solution was prepared by electrochemically exfoliating graphite rods in solution with various metal ions (KCl= 1.0 mmol L^{-1}, $NaHCO_3$ = 2.0 mmol L^{-1}, $MgSO_4$ =0.5 mmol L^{-1}, $CaCl_2$ =0.5 mmol L^{-1}) for comparison. The CDs or CDGS powder was obtained from CDs colloidal solution by freeze-drying. (MODULYOD from Thermo Fisher).

2.2. Characterizations

Zeta potential data was collected by Zeta potential – Nano particle analyzer (Delsa Nano C, BECKMAN COULTER, USA). The morphology of samples was characterized by transmission electron microscopy (TEM, Talos F200X G2). Fourier transform infrared (FT-IR) spectra were obtained on a Tensor 27 FTIR spectrometer (Nicolet 6700) with KBr as the reference sample. EPR single arising from CDs colloid solution was recorded by a Bruker EMX plus 9.5/12 spectrometer at room temperature.

2.3. Analytical methods

The concentration of Cr (VI) was detected according to the diphenyl carbamide spectrophotometry, using a UV-Vis spectrophotometer (Agilent Cary 60) at 540 nm. The concentration of Fe (II) ions, and total dissolved iron were detected according to the 1.10-phenanthroline spectrophotometry, using a UV-Vis spectrophotometer (Agilent Cary 60) at 510 nm. The fluorescence experiment was tested with a fluorospectrophotometer (Agilent Cary Eclipse). The pH values of the solution were measured by a pH meter (Metrohm Inc.). The concentrations of metal ions in solution were detected with ICP-OES instrument (Agilent ICP-OES 5110). The concentration of CDs was confirmed using a UV-Vis spectrophotometer (Agilent Cary 60) at 230 nm (Fig. S1). X-ray photoelectron spectroscopy (XPS) for elemental analysis was conducted on a Kratos Axis Ultra DLD X-ray Photoelectron Spectrometer using 60 W monochromated Mg Kα radiation as the X-ray source for excitation.

2.4. Electrochemical tests

Before each experiment, the glassy carbon electrode was cleaned in the following steps. Firstly, ultrasonic cleaning in ultrapure water and ethanol solution successively for 1 min, subsequently polished with 1.0 μm, 0.5 μm, and 0.3 μm alumina suspensions in sequence for 2 min with 8-line polishing (100 turns clockwise and 100 turns clockwise), and finally rinsed under a stream of deionized water.

Electrochemical measurements were performed on a CHI 660E electrochemical workstation (Chenhua Corp., Shanghai, China). The three-electrode system consisted of a working electrode, a platinum plate counter electrode, and an Ag/AgCl reference electrode. The potentials reported in this work were converted to the RHE scale via calibration with the following equation:

$$E(vs.RHE) = E(vs.Ag/AgCl) + 0.197 + 0.059pH \quad (1)$$

Before each measurement, the platinum counter electrode was treated by soaking in hydrochloric acid (1.0 M) to remove surface impurities. Purified N_2 gas was used to purge the oxygen from the solution for 30 min before each measurement.

3. Results and discussion

3.1. Characterizations of CDs

Different characterization methods were applied for analyzing the physicochemical properties of CDs. A stable colloid solution, whose average size is ~2.9 nm (statistics from 110 particles), was obtained with high dispersity (Fig. 1a, b). The localized sigma electrons at defects (narrow curve) and the conductive π-carriers with mobility in the aromatic graphite-like structure (broad curve) was detected by EPR (Fig. 1c), [29] which found to be the vital role in the rapid reduction process of ferric ions [24]. The functional groups were studied with FTIR analysis and latter quantified by Boehm titration [30,31]. As shown in FTIR spectrum (Fig. 1d), broad peaks at 3475 cm^{-1} and peaks at 1722, 1626, 1445, 1245 and 967 cm^{-1} are attributed to ν-OH, νC═O, νC═C, δ-OH, νC-O and γ-OH, respectively. Combined with the results of titration (Table S1), it could be known that carboxylic group (-COOH) is the main oxygen-containing functional group in CDs, indicating a high degree of oxidation on the surface sp2-hybridized C═C in aromatic ring of the CDs and formation of hydrophilic groups. Zeta potential which derives from the unique electric double layer structure of colloid was tested over a wide pH range [32]. As shown in Fig. 1e, the Zeta potential of the CDs colloid was constantly below − 40 mV over a wide pH range from 3 to 11, indicating a high dispersion resulted from stable electric layer, [33] and a considerable amount of negative charge probably caused by ionized groups (Fig. 1e, f) [34,35]. The surface defect and functional groups not only offerthe ability to act as battery (electron donor) but also the luminescence capacity [25]. The surface-related

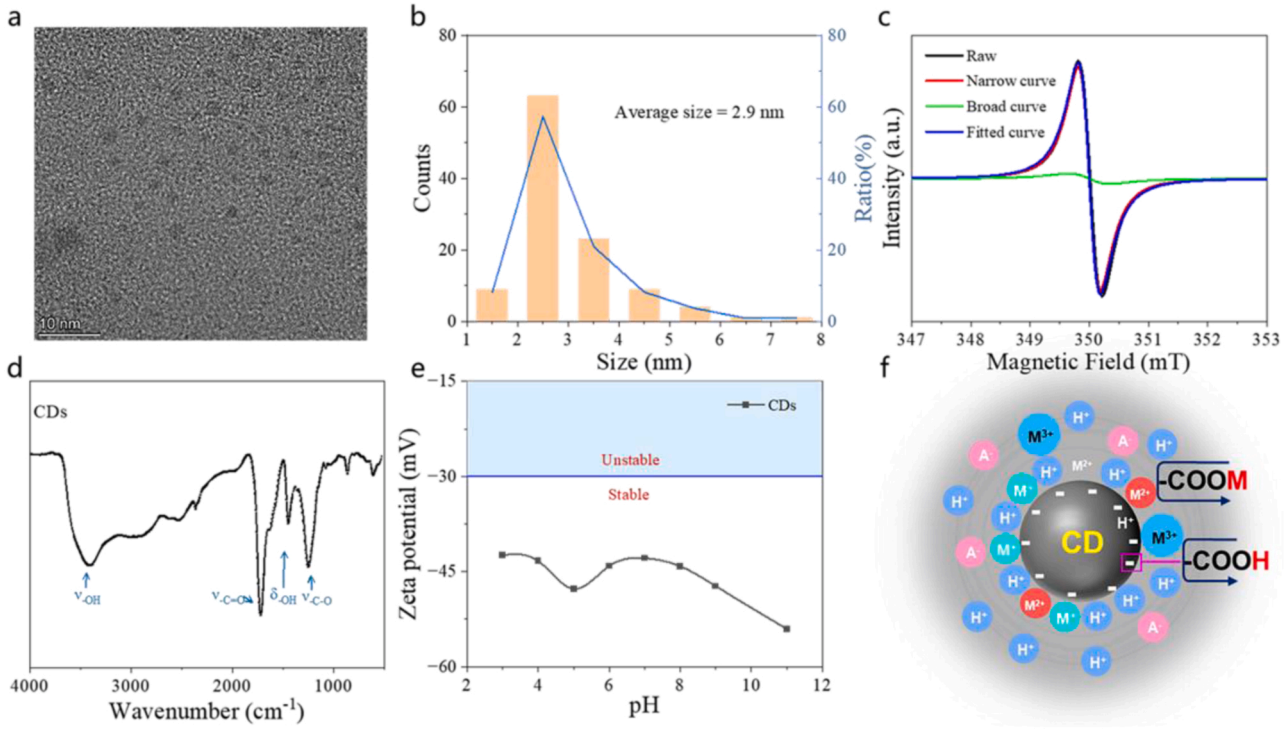

Fig. 1. (a) TEM, (b) Size distribution, (c) EPR, (d) FTIR spectrum, (e) Zeta potential, and (f) Electric double layer of CD colloid.

fluorescence signal of CDs would be quenched after the coordination to metal ions (Fig. S2).

3.2. Performance of Cr (VI) reduction on CDs

Experiments on Cr (VI) direct reduction by CDs were carried out, in which the concentration ratios of CDs and Cr (VI) were adjusted. No matter how the concentration of Cr (VI) increased, the fixed amount of

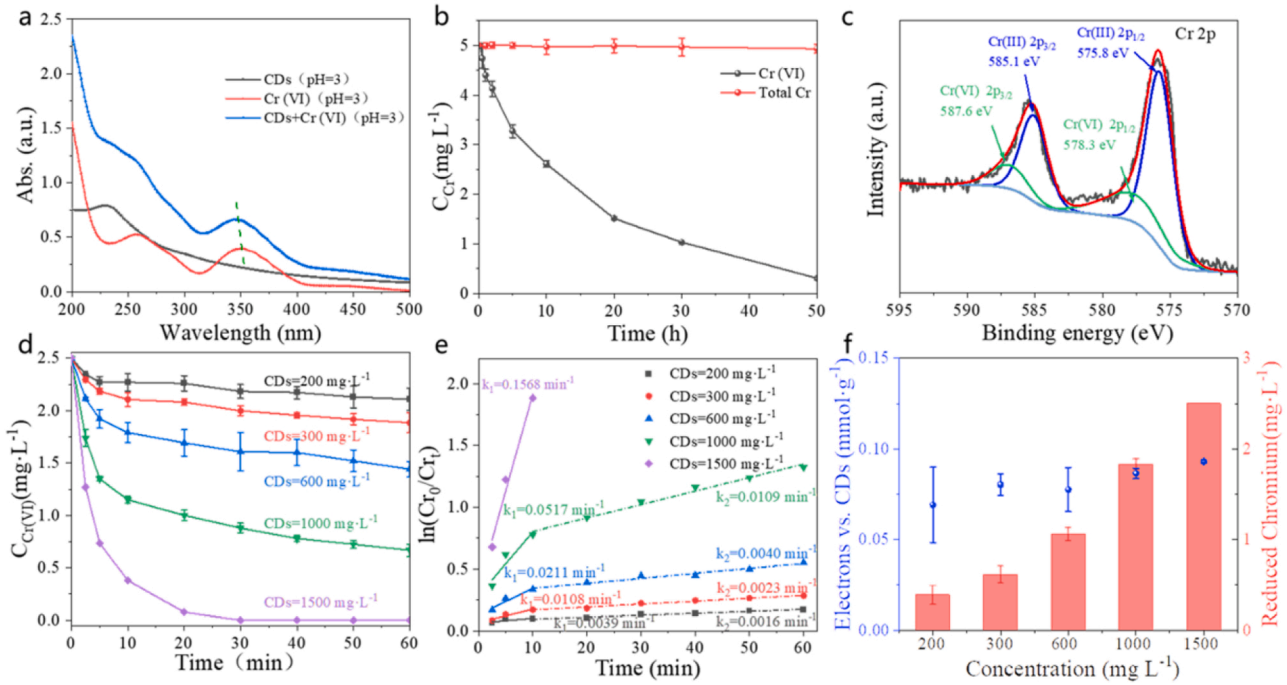

Fig. 2. The reduction performance of CDs on Cr (VI). (a) Plot of the UV-Vis spectra of Cr (VI). (b) Plot of the Cr (VI) concentration and total Cr concentration during the reduction process. (c) High-resolution XPS depth profiles of Cr 2p after reacted for 12 h. (d) Plot of $C_{Cr\ (VI)}$ versus time CDs with different concentrations. (e) Plots of $\ln(Cr_0/Cr_t)$ versus time by different concentration of CDs. (f) Electrons provided by CDs per unit mass of different samples within 20 min (left) and Cr (VI) reduced by CDs per unit mass of different samples within 1 h (right). Condition: CDs colloid solution concentration = 300 (b), 200, 300, 600, 1000, 1500 mg L^{-1} (d, e), dichromate ion concentration = 2.5 mg L^{-1}, initial pH = 3.

CDs offered close number of electrons in equal time (Fig. S3), suggesting excess Cr (VI) had no disadvantageous effect on the reduction process. As reported, the Cr (VI) could chelate with carboxyl organics (RCOOH) to construct the connection between two substances both with negative charges, achieving the electron transfer [36]. As shown in Fig. 2a, a shift occurred on the UV-Vis spectrum of Cr (VI) after adding to CDs, implying the complexation phenomenon. The total Cr was also detected, as the Cr (VI) decreased, the total Cr showed bare change during the reaction process (Fig. 2b). According to the XPS result of Cr 2p, obvious signal from Cr (III) was detected, indicating reduction of Cr(VI) to Cr(III) instead of the adsorption process (Fig. 2c) [37]. When the CDs concentration increased, the amount of reduced Cr (VI) per hour was positively correlated with the mass concentration of CDs (Fig. 2d). The number of electrons supplied per unit mass of CDs in 20 min was calculated to be in the range from 0.07 to 0.10 mmol, showing a positive correlation with the mass concentration of CDs (Fig. 2f).

The apparent rate constant was calculated and divided into two parts, both segments could have a good fit in a first-order kinetic model (k_{obs}) (Fig. 2e), demonstrating the reduction process is composed of two different reduction reactions. Two segments showed huge difference in kinetics, indicating the successively dominant role. The kinetics of first stage was obtained from 0.0039 to 0.1568 min^{-1}, while that of the second stage was only 0.0016–0.0109 min^{-1}, implying a 2–5 times difference. It is hypothesized that the two reduction pathways could be respectively attributed to the un-paired electrons from defects and surface hydroquinone-like functional groups in CDs. This speculation is in accord with previous discovery of BC owning two different electron transfer mechanisms, wherein the first part was caused by the rapid electron transfer while the second part was a result of surface oxygenic functional groups, which could last for days [22].

3.3. The effects of ions

Since the metal ions and natural organic matters are commonly found in environment, high concentrations (mass concentration = 50 mg L^{-1}) of metal ions, including K^+, Na^+, Ca^{2+}, Mg^{2+}, were respectively added to study their influence on reduction process. They all showed negligible effect on the reduction of Cr (VI) (Fig. 3a), indicating that the complexation of Cr (VI) with surface functional groups was not disturbed by the cations (K^+, Na^+, Ca^{2+}, Mg^{2+}) in water matrix and the structure of double electric layers of CD colloids was stable in the presence of these cations. The humic acid which showed long-term activity in geochemical cycle was verified in the reduction process, and showed no interference in Cr (VI) transformation (Fig. 3b). Meanwhile, the anions, including Cl^-, NO_3^-, SO_4^{2-} and HCO_3^-, were also examined and showed negligible effect on the Cr (VI) reduction (Fig. 3c). As comparison, CDSG with metal ions mentioned above displayed a more sluggish kinetics (around k_1 =2.4 ×10^{-3} min^{-1}, k_2 =7.4 ×10^{-4} min^{-1}) in the Cr (VI) reduction, which was caused by the low concentration and fewer surface functional groups (Fig. S4 and Fig. S5).

Besides the ions mentioned above, iron ions are also widespread because of the various kinds of iron ores. And trace amounts of iron ions in the environment are also generally involved in redox reactions in the geochemical cycle, which was widely investigated and proved [38]. According to the fluorescence signal of CDs in the presence of ferric ions and Cr (VI). Although both ferric ions and chromate ions showed quenching effect, there was a huge difference with an equivalent addition. Approximately 30 times the molar amount of chromate ion was required to achieve a similar quenching effect as the ferric ions (Fig. S6), indicating CDs preferred to interact with iron, which was realized through the carboxyl group via bidentate [39]. It could be inferred that, coordination occurred on CDs with both iron and Cr (VI), but the negative charge and electric double layer led to a lower possibility in Cr

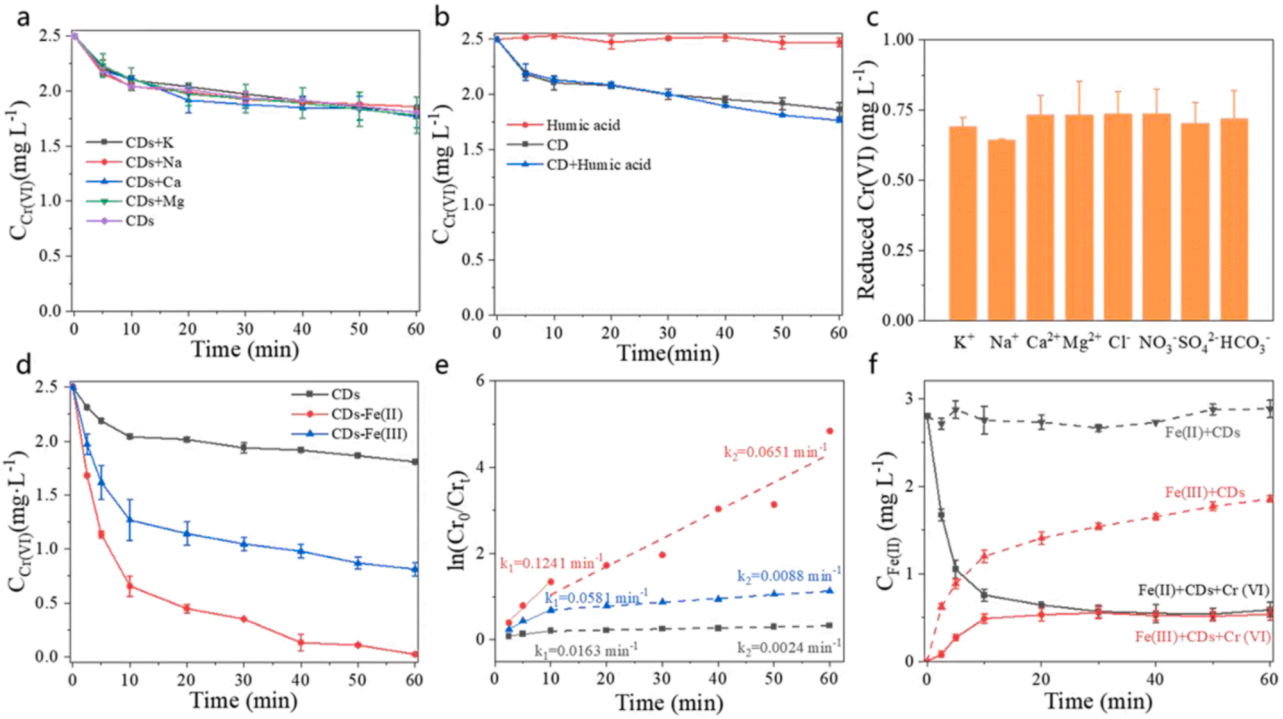

Fig. 3. The reduction performance of CDs in the presence of other ions. (a) Plot of the $C_{Cr\ (VI)}$ versus time by CDs with K^+, Na^+, Ca^{2+} and Mg^{2+}, respectively. (b) Plot of the $C_{Cr\ (VI)}$ versus time by CDs with humic acid. (c) Plots of reduced Cr (VI) by CDs with different ions, including K^+, Na^+, Ca^{2+} Mg^{2+}, Cl^-, NO_3^-, SO_4^{2-} and HCO_3^- in 1 h. (d) Plot of the $C_{Cr\ (VI)}$ versus time by CDs with ferric ions and ferrous ions, respectively. (e) Plot of $\ln(Cr_0/Cr_t)$ versus time by CDs with ferric ions and ferrous ions, respectively. (f) Plot of the $C_{Fe(II)}$ versus time by CDs and Cr (VI). Condition: CDs colloid solution concentration = 300 mg L^{-1}, concentration of K^+, Na^+, Ca^{2+} Mg^{2+}, Cl^-, NO_3^-, SO_4^{2-} and HCO_3^- are all 50 mg L^{-1}, concentration of added ferric ions and ferrous ions are both 2.8 mg L^{-1}, dichromate ion concentration = 2.5 mg L^{-1}, initial pH = 3.

(VI) coordination. Despite the straightforward reduction process of ferric ions by CDs, it deserves to determine whether the reduction of Cr (VI) would be disturbed by strongly concatenated ferric ions and whether there is competition for electrons.

In view of the reducing property on Cr (VI) from ferrous ions, [40] controlled experiments were carried out, demonstrating little influence from iron ions on both reduction process and detection process (Fig. S7). In other word, electrons from Fe (II) were unable to deliver to Cr (VI) under this condition, despite the relatively low redox potential of Fe^{3+}/Fe^{2+} (0.77 V) comparing to Cr^{6+}/Cr^{3+} (1.33 V). After the addition of Fe (II) or Fe (III) to CDs colloidal solution, not only did the Fe (II) promote the reduction of Cr (VI), but also the addition of Fe (III) promoted the reduction effect of Cr (VI) (Fig. 3d, e). This phenomenon indicated the coordination of iron availed for Cr (VI) reduction instead of competing for electrons, and the Fe(II) or Fe(III) ions chelating with -COOH may act as the electron tunnels for Cr (VI) reduction [39,41].

Comparing with the original data without the addition of ferric ions, it can be found that the reduction increased to 2.5 times within ten minutes after the addition of Fe (III), the kinetics rate increased to 4 times within ten minutes after the addition of Fe (II). And within one hour, the reduction amount increased to 3 times after the addition of Fe (III), while the addition of Fe (II) achieved complete reduction of Cr (VI). As a more significant increasement was witnessed, suggesting the reduction pathway of functional groups was more likely to be affected by the addition of iron ions. After the addition of different concentrations of Fe (II) or Fe (III), a positive relation was witnessed between reduced Cr (VI) and added iron (Fig. S8). The variation tendency of iron ions after addition was examined (Fig. S9) and collected (Fig. 3f). The Fe (II) concentration was constantly kept at ~0.5 mg L^{-1} during the process, comparing to the gradual increase in Fe (II) without Cr (VI). These results showed that iron ions act as a good electron transfer medium during the reduction process rather than simply changing the electron transfer properties of CDs, which might be achieved through the function between chromium and oxygen connected iron [42].

As for CDSG, the reduction process was likewise improved by the addition of iron ions. Even if the CDs were coordinated with surrounding abundant metal cations during electrolysis, the CD-COOFe complex structure was still formed for the removal of Cr (VI), indicating the prior interaction between iron ions (Fe (II) or Fe (III)) and CDs (Fig. S10).

3.4. Diffusion constant and electron transfer rate constant

Electrochemical analysis was employed to have a better understanding of the reduction mechanism, by constructing a three-electrode system with CD electrolyte. Two pairs of redox peaks appeared in the cyclic voltammogram, representing two quasi-reversible processes (both single-electron transfer electrochemical redox processes), corresponding to reduction experiments in which exists two different reduction mechanisms (Fig. 3a). The oxidation peak potential (Ep, c1) and reduction peak potential (Ep, a1) for redox reaction 1 are 0.344 V and 0.405 V, respectively. Oxidation peak potential (Ep, c2) and reduction peak potential (Ep, a2) for redox reaction 2 are 0.502 V and 0.568 V, respectively. According to previous studies, the reduction potential of quinone-hydroquinone pairs on carbon materials is about 0.5–0.55 V [43]. Therefore, the redox reaction 2 of the CDs originates from the redox behavior of the quinone group, whereas the redox reaction 1 should be related to the redox process of unpaired spin electrons [39]. The larger peak potential difference for redox reaction 2 indicates that the transfer of electrons dominated by the surface functional groups would be more difficult than that dominated by the unpaired electrons, which could be owing to electrostatic effects, consistent with the actual experimental results of the larger kinetic differences between the two different reduction mechanisms [44]. With the increasement in the sweep speed, progressively more pronounced peak for redox reaction 1 and a progressively flatter redox reaction 2 were observed. The difference was speculated from the distinction in electron transfer pathway. Redox reaction 1 is able to occur rapidly due to the increased sweep speed and the increased frequency of contact between the electrode and the CD colloid, resulting in a more pronounced signal response at the electrode surface, whereas the redox reaction 2 resulted from quinone-hydroquinone functional group reacts relatively slowly. Increasing the sweep speed led to a reduction on the contact time between the electrode surface and the CDs, and thus the signal was weakened.

In the further quantitative analysis, Randles-Sevcik equation and Nicholson equation were applied to this quasi-reversible redox system to calculate diffusion coefficients and electron transfer rate constants for the CDs after the introduction of metal ions (Table 1). For the electrochemical electron transfer process involving freely diffusing redox species, the Randles-Sevcik equation describes the relationship (Fig. 3b) between i_p and the square root of the scan rate ν (V s^{-1})

$$i_p = 0.4463nFAC\left(\frac{nF\nu D}{RT}\right)^{0.5} \quad (2)$$

where i_p, n, A, F, D, ν, R and T are the peak current (mA), electron transfer number, electrode area (cm^2), Faraday constant (96,485 C mol^{-1}), diffusion coefficient (10^{-5} cm^2 s^{-1}), scan rate (V s^{-1}), gas constant (8.314 J K^{-1} mol^{-1}) and temperature (K), respectively.

And the standard rate constants for quasi-reversible redox systems could be determined by Nicholson equation, in which ΔEp is a function of a dimensionless kinetic parameter(ψ) (Fig. 3c). The only requirements for using Nicholson's method are the measurement of ΔEp at different scan rates, followed by the determination of the corresponding values of ψ via equation [45,46].

$$\psi = \frac{(-0.6288 + 0.0021\Delta E_p)}{1 - 0.017\Delta E_p} \quad (3)$$

where ΔEp is the difference between potential of oxidation peak and reduction peak in a redox pair.

Following Nicholson's working curve, the rate constant can thus be calculated by equation (Fig. 3d)

$$k^0 = \frac{k_n}{\sqrt{RT/\pi nFD}} \quad (4)$$

where k^0, k_n, R, T, n F and D are the electron transfer rate constant (cm s^{-1}), slope obtained from a linear fit of the relationship between Ψ and $v^{-0.5}$, gas constant (8.314 J K^{-1} mol^{-1}) and temperature (K), number of the electron transfer, Faraday constant (96,485 C mol^{-1}), and diffusion coefficient, respectively.

Compared to the potassium ferricyanide ion in the control experiment (diffusion coefficient of approximately 0.63 $\times 10^{-5}$ cm^2 s^{-1}), the diffusion coefficient of the CDs is an order of magnitude smaller, indicating the difficulty in migration comparing to ions. And the addition of high concentration (100 mg L^{-1}) of K^+ and Ca^{2+} and reactive metal ions (10 mg L^{-1}) had a small effect on the diffusivity of CDs as well as surface charge. In another hand, results of the Nicholson equation show that the addition of K^+ and Ca^{2+} had slight influence on the electron transfer, while the addition of Fe (III) offered a huge promotion and Cr (VI) showed a significant obstacle. The decrease in electron transfer constant

Table 1
Electrochemical data calculated according to Randles-Sevcik equation and Nicholson equation (Fig. S11-14).

Parameter	CDs	CDs+K^+	CDs+Ca^{2+}	CDs+Fe^{3+}	CDs+Cr (VI)
Diffusion constant (10^{-5} cm^2 s^{-1})	0.01068	0.01067	0.01193	0.01073	0.01058
Electron transfer rate constant (10^{-3} cm s^{-1})	6.94	6.84	8.05	10.00	4.98

represented more electrons shifting between CDs and Cr (VI) rather than between CDs and the glassy-carbon electrode, which is accord with previous reduction performance of CDs in the presence of metal ions. (fig. 4).

3.5. The effect of pH values

Throughout the system, changes in pH not only alter the form of Cr (VI), but also have an effect on the double electric layer surrounding the CDs, making it crucial to understand the effect of pH. It was found that the reduction pathway controlled by functional groups was more susceptible to the proton concentration, slightly hindered in neutral condition, almost stalled in strongly alkaline situations (Fig. 5a, b). After addition of iron ions, the inference was especially evident (Fig. 5c, d). Although reduction still proceeded, the reduction potential was decreased more than 50 %. The significant effect from pH was presumably because the protons in the solution are closely involved in the reduction process. Previous studies have shown that the reduction of Fe^{3+} were influenced by the protons around the microenvironment of the complex structure [39]. In addition, the concentration of protons also affects the structure of the double electric layer on the surface of CD and the form of Cr (VI). In alkaline solutions, the Cr (VI) is no longer predominantly in the form of $Cr_2O_7^{2-}$, but in the form of CrO_4^{2-}. There are differences between dichromate and chromate in complexing with surface oxygen functional groups [47]. As shown in the equation, the oxidation of Cr (VI) in alkaline environments is much harder than in acidic conditions, thus leading to a slower reduction process. In addition, under alkaline conditions, there are fewer cations around the CD and the outer anions are more difficult to approach the carbon nanodots due to electrostatic effects.

$$Cr_2O_7^{2-} + 14H^+ + 6e^- \rightarrow 2Cr^{3+} + 7H_2O \varepsilon_0 = 1.33V \quad (5)$$

$$CrO_4^{2-} + 4H_2O + 3e^- \rightarrow Cr(OH)_3 + 5OH^- \varepsilon_0 = -0.13V \quad (6)$$

3.6. Mechanism

The CDs colloids showed a unique electric double layer which was surrounded tightly by cations nearby and acted as the center of incompact anions. The Cr (VI) could be chelated with -COOH on CDs, affected by the electric double layer. The driving force of reduction from Cr (VI) to Cr (III) were the carbon defects (un-paired electrons in the sp^2 carbon matrix) and surface functional groups, which respectively dominated different reduction reactions. A complex structure of surface carboxylic acid chelating with Fe^{2+} or Fe^{3+} ions were stably formed. This complex structure provided the opportunity to donor the electrons more rapidly through the iron-oxygen-chromium pathway. The direct reduction of Cr (VI) by CDs, which was supported thermodynamically and hindered kinetically, was improved by the intermediated process of ferric ions reduction. The complex structure of CDs with Fe^{2+} or Fe^{3+} ions promoted the electron transfer during the reduction process of Cr (VI). However, the effect of metal cations such as (K^+, Na^+, Ca^{2+} and Mg^{2+}) and anions (including Cl^-, NO_3^-, SO_4^{2-} and HCO_3^-) on direct reduction of Cr (VI) on CDs were negligible. (fig. 6).

4. Conclusion

The mechanism of reduction process of Cr (VI) was explored in the presence of common ions of the water matrix by CDs with defects and surface oxygen functional groups as a simple constitute units of carbonaceous materials. The Cr (VI) could be directly reduced by CDs with

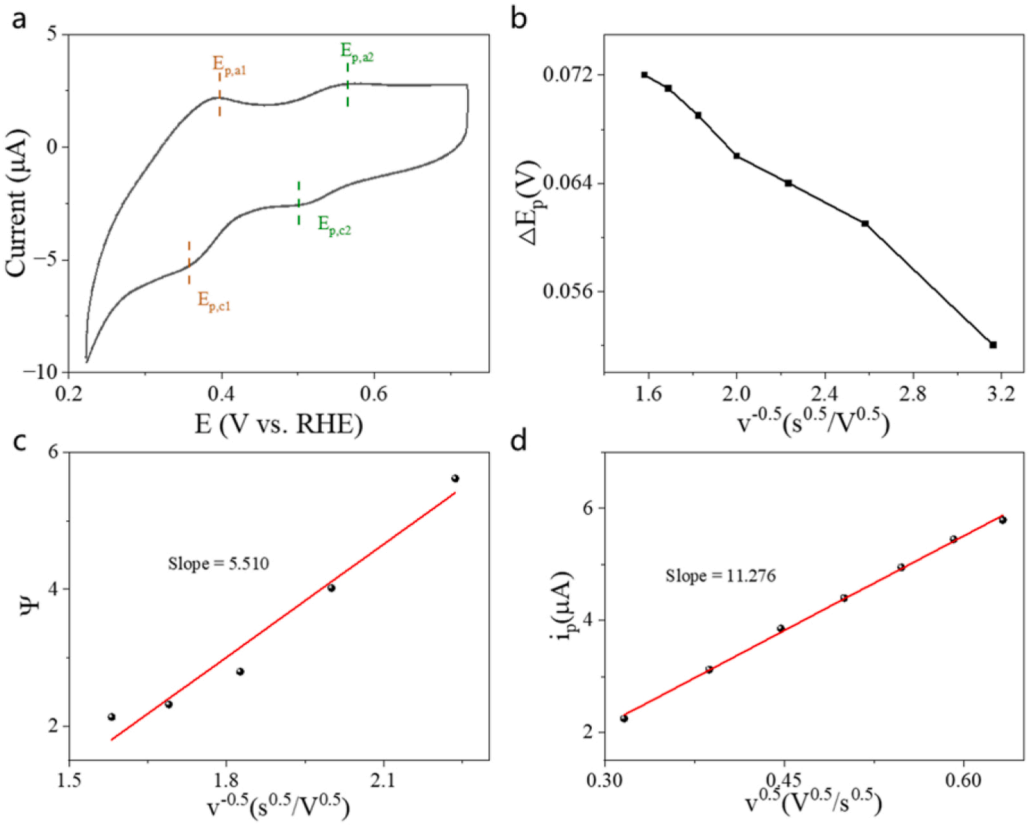

Fig. 4. Electrochemical curve, Randles-Sevcik equation process and Nicholson equation process. (a) Cyclic voltammogram curves of CDs colloidal solution measured in the absence of O_2. Relationship of (b) $\triangle Ep \sim v^{-0.5}$, (c) $\Psi \sim v^{-0.5}$ and (d) $i_p \sim v^{0.5}$ from which k^0 was calculated for CDs colloidal solution. Condition: CDs concentration = 2500 mg L^{-1}, scan rate of 100–400 mV s^{-1}, pH = 2.7.

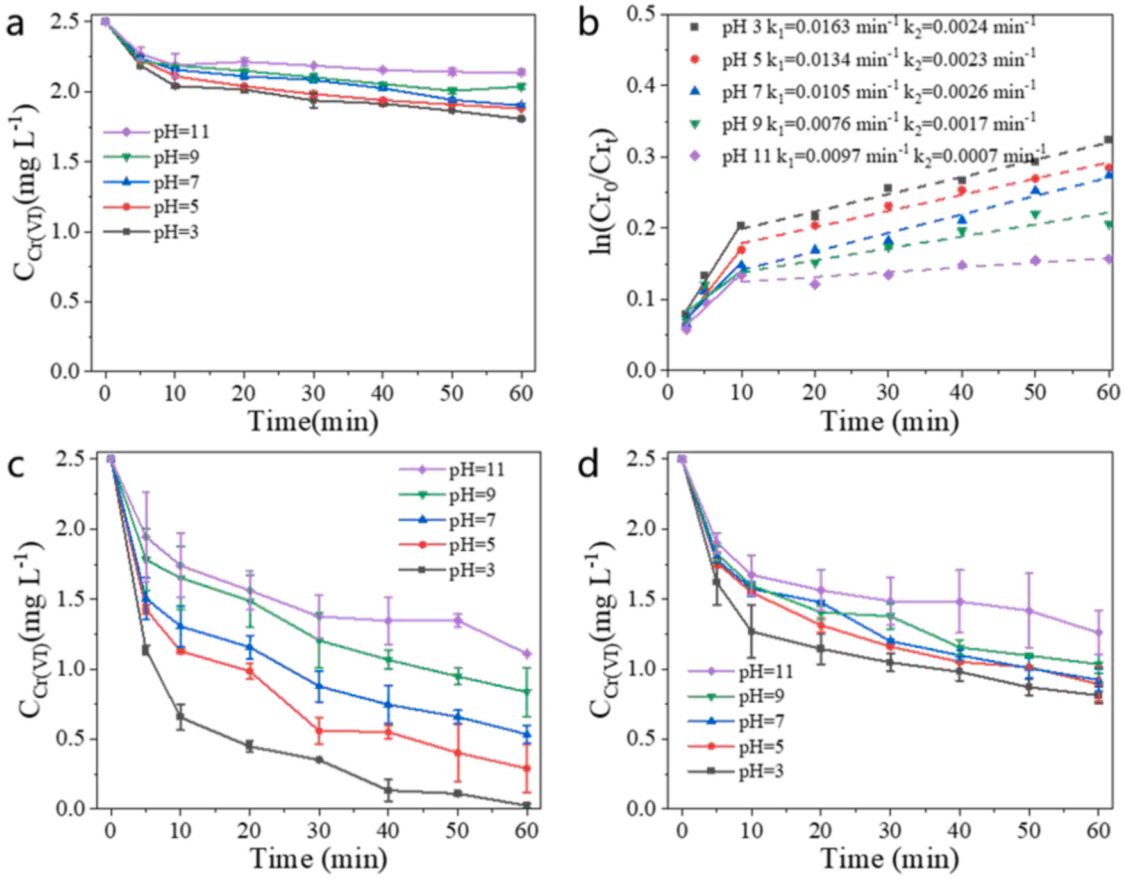

Fig. 5. The reduction performance of CDs and CD-COOFe on Cr (VI) at different pH. (a) Plot of $C_{Cr\ (VI)}$ versus time in reduction of Cr by CDs in different pH values. (b) Plots of ln(Cr_0/Cr_t) versus time by CDs in different pH, (c) Plot of $C_{Cr\ (VI)}$ versus time in reduction of Cr by CDs-COOFe(II) in different pH values. (d) Plot of $C_{Cr\ (VI)}$ versus time in reduction of Cr by CDs-COOFe(III) in different pH values. Condition: CD colloid solution concentration = 300 mg L^{-1}, concentration of added ferric ions and ferrous ions are both 2.8 mg L^{-1}, dichromate ion concentration = 2.5 mg L^{-1}.

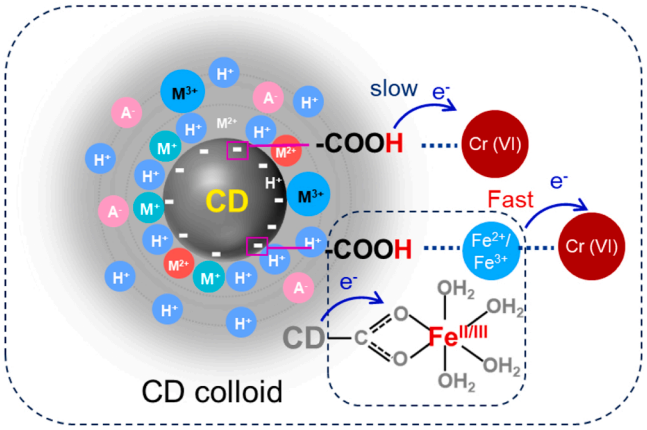

Fig. 6. Mechanism of the reduction pathway of Cr (VI) on CD colloid with defects and surface oxygen functional groups.

carboxylic acid groups interacting via chelation. The electron donated by CDs to reduce Cr (VI) was calculated and it is dependent on the mass concentration of CDs colloids. The above process is stable and independent of ambient ions around the double electric layer of CDs colloids, but suppressed by the decreased concentration of protons. The reduction process is well differentiated into two primary kinetic processes, of which the first being dominated by the unpaired electrons of carbon defects and the second by the oxygen functional groups on the surface. The Fe^{2+} or Fe^{3+} cations interaction with CDs by chelation would promote electron transfer process, acting as a medium for Cr (VI) reduction. This work lays out valuable guidelines for further exploration of the redox behaviors of carbonaceous materials such as BC etc. in the natural environment.

CRediT authorship contribution statement

Zhelun Pan: Writing – original draft, Validation, Formal analysis, Visualization, Investigation. **Ting Zhang:** Writing – review & editing, Validation, Formal analysis, Visualization, Methodology, Investigation. **Xufang Qian:** Methodology, Writing – review & editing, Funding acquisition, Resources, Supervision, Project administration, Investigation. **Yixin Zhao:** Funding acquisition, Resources, Supervision, Project administration.

Declaration of Competing Interest

The authors declare that they have no known competing financial interests or personal relationships that could have appeared to influence the work reported in this paper.

Data Availability

The authors do not have permission to share data.

Acknowledgments

We gratefully acknowledge the support of the National Natural Science Foundation of China (22276123), the Ministry of Science and Technology of China (2021YFA1201701, 2018YFC1802001), the Shanghai Engineering Research Center of Water Environment Simulation and Ecological Restoration (WESER-202201). We thank the Instrumental Analysis Center (School of Environmental Science and Engineering and Shanghai Jiao Tong University) for assistance with material characterization tests.

Appendix A. Supporting information

Supplementary data associated with this article can be found in the online version at doi:10.1016/j.apcatb.2023.122571.

References

[1] Y. Ding, Z.A. Qiao, Carbon surface chemistry: new insight into the old story, Adv. Mater. 34 (2022), e2206025.
[2] Y. Jia, L. Zhang, L. Zhuang, H. Liu, X. Yan, X. Wang, J. Liu, J. Wang, Y. Zheng, Z. Xiao, E. Taran, J. Chen, D. Yang, Z. Zhu, S. Wang, L. Dai, X. Yao, Identification of active sites for acidic oxygen reduction on carbon catalysts with and without nitrogen doping, Nat. Catal. 2 (2019) 688–695.
[3] C. Tang, H.F. Wang, X. Chen, B.Q. Li, T.Z. Hou, B. Zhang, Q. Zhang, M.M. Titirici, F. Wei, Topological defects in metal-free nanocarbon for oxygen electrocatalysis, Adv. Mater. 28 (2016) 6845–6851.
[4] Y. Jiang, L. Yang, T. Sun, J. Zhao, Z. Lyu, O. Zhuo, X. Wang, Q. Wu, J. Ma, Z. Hu, Significant contribution of intrinsic carbon defects to oxygen reduction activity, ACS Catal. 5 (2015) 6707–6712.
[5] Y. Jia, L. Zhang, A. Du, G. Gao, J. Chen, X. Yan, C.L. Brown, X. Yao, Defect graphene as a trifunctional catalyst for electrochemical reactions, Adv. Mater. 28 (2016) 9532–9538.
[6] I.L. Li, Z.K. Tang, Curvature effect in ultra-small single-walled carbon nanotubes, Appl. Surf. Sci. 226 (2004) 72–77.
[7] G.L. Luque, M.I. Rojas, E.P.M. Leiva, Curvature effect in the longitudinal unzipping carbon nanotubes, J. Solid State Electrochem. 17 (2013) 1189–1200.
[8] H. Zhao, C. Sun, Z. Jin, D.-W. Wang, X. Yan, Z. Chen, G. Zhu, X. Yao, Carbon for the oxygen reduction reaction: a defect mechanism, J. Mater. Chem. A 3 (2015) 11736–11739.
[9] N. Brown, O. Hod, Controlling the electronic properties of nanodiamonds via surface chemical functionalization: a DFT study, J. Phys. Chem. C 118 (2014) 5530–5537.
[10] S. Adil, W.S. Kim, T.H. Kim, S. Lee, S.W. Hong, E.J. Kim, Defective, oxygen-functionalized multi-walled carbon nanotubes as an efficient peroxymonosulfate activator for degradation of organic pollutants, J. Hazard. Mater. 396 (2020), 122757.
[11] Z. Yang, J. Qian, A. Yu, B. Pan, Singlet oxygen mediated iron-based Fenton-like catalysis under nanoconfinement, Proc. Natl. Acad. Sci. USA 116 (2019) 6659–6664.
[12] X. Duan, H. Sun, Y. Wang, J. Kang, S. Wang, N-doping-induced nonradical reaction on single-walled carbon nanotubes for catalytic phenol oxidation, ACS Catal. 5 (2014) 553–559.
[13] W. Ren, G. Nie, P. Zhou, H. Zhang, X. Duan, S. Wang, The intrinsic nature of persulfate activation and N-doping in carbocatalysis, Environ. Sci. Technol. 54 (2020) 6438–6447.
[14] P.J.C. Wolfgang, Seiler Estimates of gross and net fluxes of carbon between the biosphere and the atmosphere from biomass burning, Clim. Change 2 (1980) 41.
[15] G.J.J. Smith, D.M. Goldberg, E.D. Goldberg, Elemental carbon in marine sediments: a baseline for burning, Nature 241 (1973) 268–270.
[16] C.P.J. Kuhlbusch, T.A.J. Black, carbon, the global carbon cycle, and atmospheric carbon dioxide, Biomass Burn. Glob. Change (1996) 10.
[17] A. Stubbins, J. Niggemann, T. Dittmar, Photo-lability of deep ocean dissolved black carbon, Biogeosciences 9 (2012) 1661–1670.
[18] T. Dittmar, C.E. De Rezende, M. Manecki, J. Niggemann, A.R. Coelho Ovalle, A. Stubbins, M.C. Bernardes, Continuous flux of dissolved black carbon from a vanished tropical forest biome, Nat. Geosci. 5 (2012) 618–622.
[19] S.W. Alysha, I. Coppola, Sinikka T. Lennartz, Michael Seidel, Ward Nicholas, D. Thorsten Dittmar, Cristina Santín, Matthew W. Jones, The black carbon cycle and its role in the Earth system, Nat. Rev. Earth Environ. (2022).
[20] Y. Zhang, X. Xu, L. Cao, Y.S. Ok, X. Cao, Characterization and quantification of electron donating capacity and its structure dependence in biochar derived from three waste biomasses, Chemosphere 211 (2018) 1073–1081.
[21] W. Liang, C.E. Bunker, Y.P. Sun, Carbon dots: zero-dimensional carbon allotrope with unique photoinduced redox characteristics, ACS Omega 5 (2020) 965–971.
[22] T. Sun, B.D. Levin, J.J. Guzman, A. Enders, D.A. Muller, L.T. Angenent, J. Lehmann, Rapid electron transfer by the carbon matrix in natural pyrogenic carbon, Nat. Commun. 8 (2017) 14873.
[23] A. Bhati, S.R. Anand, D. Saini, Gunture, S.K. Sonkar, Sunlight-induced photoreduction of Cr(VI) to Cr(III) in wastewater by nitrogen-phosphorus-doped carbon dots, npj Clean Water 2 (2019).
[24] T. Zhang, Y. Wen, Z. Pan, Y. Kuwahara, K. Mori, H. Yamashita, Y. Zhao, X. Qian, Overcoming acidic H_2O_2/Fe(II/III) redox-induced low H_2O_2 utilization efficiency by carbon quantum dots Fenton-like catalysis, Environ. Sci. Technol. 56 (2022) 2617–2625.
[25] L. Bao, Z.-L. Zhang, Z.-Q. Tian, L. Zhang, C. Liu, Y. Lin, B. Qi, D.-W. Pang, Electrochemical tuning of luminescent carbon nanodots: from preparation to luminescence mechanism, Adv. Mater. 23 (2011) 5801–5806.
[26] D. Mohan, C.U. Pittman, Activated carbons and low cost adsorbents for remediation of tri- and hexavalent chromium from water, J. Hazard. Mater. 137 (2006) 762–811.
[27] U.Y. Stambulska, M.M. Bayliak, V.I. Lushchak, Chromium(VI) toxicity in legume plants: modulation effects of Rhizobial symbiosis, BioMed. Res. Int. 2018 (2018) 8031213.
[28] H. Ming, Z. Ma, Y. Liu, K. Pan, H. Yu, F. Wang, Z. Kang, Large scale electrochemical synthesis of high quality carbon nanodots and their photocatalytic property, Dalton Trans. 41 (2012) 9526–9531.
[29] Y. Chong, C. Ge, G. Fang, X. Tian, X. Ma, T. Wen, W.G. Wamer, C. Chen, Z. Chai, J. J. Yin, Crossover between anti- and pro-oxidant activities of graphene quantum dots in the absence or presence of light, ACS Nano 10 (2016) 8690–8699.
[30] R.B. Fidel, D.A. Laird, M.L. Thompson, Evaluation of modified boehm titration methods for use with biochars, J. Environ. Qual. 42 (2013) 1771–1778.
[31] M.S. Alam, D. Gorman-Lewis, N. Chen, S. Safari, K. Baek, K.O. Konhauser, D. S. Alessi, Mechanisms of the removal of U(VI) from aqueous solution using biochar: a combined spectroscopic and modeling approach, Environ. Sci. Technol. 52 (2018) 13057–13067.
[32] S. Bhattacharjee, DLS and zeta potential – what they are and what they are not? J. Control. Release 235 (2016) 337–351.
[33] A. Kumar, C.K. Dixit, Methods for characterization of nanoparticles, in: S. Nimesh, R. Chandra, N. Gupta (Eds.), Advances in Nanomedicine for the Delivery of Therapeutic Nucleic Acids, Woodhead Publishing, 2017, pp. 43–58.
[34] D. Li, M.B. Muller, S. Gilje, R.B. Kaner, G.G. Wallace, Processable aqueous dispersions of graphene nanosheets, Nat. Nanotechnol. 3 (2008) 101–105.
[35] B. Konkena, S. Vasudevan, Understanding aqueous dispersibility of graphene oxide and reduced graphene oxide through pKa measurements, J. Phys. Chem. Lett. 3 (2012) 867–872.
[36] X. Gao, Y. Zhang, F. Li, B. Tian, X. Wang, Z. Wang, J.C. Carozza, Z. Zhou, H. Han, C. Xu, Surface modulation and chromium complexation: all-in-one solution for the Cr(VI) sequestration with bifunctional molecules, Environ. Sci. Technol. 54 (2020) 8373–8379.
[37] L. Tang, G.-D. Yang, G.-M. Zeng, Y. Cai, S.-S. Li, Y.-Y. Zhou, Y. Pang, Y.-Y. Liu, Y. Zhang, B. Luna, Synergistic effect of iron doped ordered mesoporous carbon on adsorption-coupled reduction of hexavalent chromium and the relative mechanism study, Chem. Eng. J. 239 (2014) 114–122.
[38] S. Xu, D. Adhikari, R. Huang, H. Zhang, Y. Tang, E. Roden, Y. Yang, Biochar-facilitated microbial reduction of hematite, Environ. Sci. Technol. 50 (2016) 2389–2395.
[39] T. Zhang, Z. Pan, J. Wang, X. Qian, H. Yamashita, Z. Bian, Y. Zhao, Homogeneous carbon dot-anchored Fe(III) catalysts with self-regulated proton transfer for recyclable Fenton chemistry, JACS Au (2023), https://doi.org/10.1021/jacsau.2c00644.
[40] M.A. Schlautman, I. Han, Effects of pH and dissolved oxygen on the reduction of hexavalent chromium by dissolved ferrous iron in poorly buffered aqueous systems, Water Res. 35 (2001) 1534–1546.
[41] L. Wang, M. Cao, Z. Ai, L. Zhang, Design of a highly efficient and wide pH electro-Fenton oxidation system with molecular oxygen activated by ferrous-tetrapolyphosphate complex, Environ. Sci. Technol. 49 (2015) 3032–3039.
[42] D.C.G. John, M. Zachara, Ronald L. Schmidt, C. Thomas Resch, Chromate adsorption on amorphous iron oxyhydroxide in the presence of major groundwater ions, Environmental Science and Technology 21 (1987) 589–594.
[43] G.-F. Han, F. Li, W. Zou, M. Karamad, J.-P. Jeon, S.-W. Kim, S.-J. Kim, Y. Bu, Z. Fu, Y. Lu, S. Siahrostami, J.-B. Baek, Building and identifying highly active oxygenated groups in carbon materials for oxygen reduction to H2O2, Nat. Commun. 11 (2020) 2209.
[44] J. Phelps, A.J. Bard, One- vs. two-electron oxidations of tetraarylethylenes in aprotic solvents, J. Electroanal. Chem. Interfacial Electrochem. 68 (1976) 313–335.
[45] I. Lavagnini, R. Antiochia, F. Magno, An extended method for the practical evaluation of the standard rate constant from cyclic voltammetric data, Electroanalysis 16 (2004) 505–506.
[46] H. Wang, S.Y. Sayed, E.J. Luber, B.C. Olsen, S.M. Shirurkar, S. Venkatakrishnan, U. M. Tefashe, A.K. Farquhar, E.S. Smotkin, R.L. McCreery, J.M. Buriak, Redox flow batteries: how to determine electrochemical kinetic parameters, ACS Nano 14 (2020) 2575–2584.
[47] F. Brito, J. Ascanio, S. Mateo, C. Hernández, L. Araujo, P. Gili, P. Martín-Zarza, S. Domínguez, A. Mederos, Equilibria of chromate(VI) species in acid medium and ab initio studies of these species, Polyhedron 16 (1997) 3835–3846.